

# PIEZOELECTRIC/MAGNETOSTRICTIVE MEMS RESONANT SENSOR ARRAY FOR IN-PLANE MULTI-AXIS MAGNETIC FIELD DETECTION

Hoe Joon Kim<sup>1,2</sup>, Sibong Wang<sup>1,3</sup>, Changting Xu<sup>1</sup>, David Laughlin<sup>1</sup>, Jingxi Zhu<sup>3,4</sup>, and Gianluca Piazza<sup>1</sup>

<sup>1</sup>Carnegie Mellon University, Pittsburgh, USA

<sup>2</sup>Daegu Gyeongbuk Institute of Science and Technology (DGIST), Daegu, South Korea

<sup>3</sup>Sun Yat-sen University, Guangzhou, China

<sup>4</sup>Sun Yat-Sen University-Carnegie Mellon University Shunde International Joint Research Institute, Guangdong, China

## ABSTRACT

This paper reports the demonstration of an array of piezoelectric/magnetostrictive micro electromechanical system (MEMS) magnetic resonant sensors (PM-MRS) for multi-axis magnetic field (H-field) detection. An array of 43 MHz aluminum nitride (AlN) piezoelectric resonators vibrating along different in-plane directions ( $\theta$ ) but coated with a magnetostrictive layer ( $\text{Fe}_{65.6}\text{Co}_{9.4}\text{B}_{25}$ ) with the same easy axis (EZ) exhibit unique mechanical/ electrical responses as a function of the applied H-field and its direction, enabling a high resolution multi-axis H-field detection. The sensor design yields resonators with a high quality factor ( $Q \sim 1500$ ) and electromechanical coupling coefficient ( $k_t^2 \sim 2\%$ ) – the highest value ever reported for an AlN PM-MRS. This sensor system paves the way for low power magnetometers that enables single-chip multi-axis H-field detection.

## INTRODUCTION

Compact, power efficient, and highly sensitive magnetometers are crucial in building the next generation of electronic compasses and navigation systems. Recently developed solid-state magnetometers and resonant MEMS magnetic sensors utilizing Lorentz force [1-4] or piezoresistive/ magnetostrictive composites [5-7] show high sensitivity and measurement resolution while fully compatible with CMOS technology.

MEMS magnetometers based on Lorentz force can measure H-field in 3-axis, but require a significant amount of power, up to tens-of-mW, for sensor actuation [1-4]. In contrast, recently developed PM-MRS [5-7] do not require an active current to detect magnetic fields, hence enabling low power H-field detection. Moreover, PM-MRS provide high measurement resolution as the Young's modulus ( $E$ ) of the integrated magnetostrictive layer is a strong function of the applied H-field (delta-E effect [8]). Such shift in  $E$  could be as large as 30%, depending on the amount of H-field and its direction, inducing a large modulation in sensor center frequency ( $f_0$ ) [9]. However, previously demonstrated PM-MRS are not yet capable of monolithic multi-axis detection, as they require the use of either multiple chips or multiple depositions of magnetostrictive materials with different easy axis (EZ) directions.

In this work, we demonstrate a design, fabrication, characterization and application of monolithic array of PM-MRS with different excitation orientations to more accurately detect H-field orientation and its magnitude.

## SENSOR DESIGN, FABRICATION, AND CHARACTERIZATION

The PM-MRS of this work measures H-field intensity by monitoring changes in the resonant frequency ( $f_0$ ) of the sensor caused by variations in the  $E$  of the magnetostrictive material when exposed to H-field. Figure 1(a) shows a cross sectional view of the resonant sensor. A piezoelectric layer (AlN) is sandwiched between top signal (Al) and bottom ground (Pt) electrodes. Electric field generated between the electrodes induces lateral vibration of AlN. The width of the resonator ( $w$ ) sets  $f_0$ :

$$f_0 = \frac{1}{2w} \sqrt{\frac{E_{eq}}{\rho_{eq}}} \quad (1)$$

$$E_{eq} = \frac{E_{AlN}t_{AlN} + E_{Pt}t_{Pt} + E_{FeCoB}t_{FeCoB}}{t_{AlN} + t_{Pt} + t_{FeCoB}} \quad (2)$$

where  $E_{eq}$  and  $\rho_{eq}$  are equivalent Young's modulus and equivalent density of the resonator and  $t$  is the thickness of each layer forming the resonator stack. Although an approximation, Eq. (2) provides a good description of the main parameter that varies in the presence of a magnetic field. When the H-field is applied, the delta-E effect of FeCoB changes  $E_{eq}$ , and thus shifts  $f_0$ .

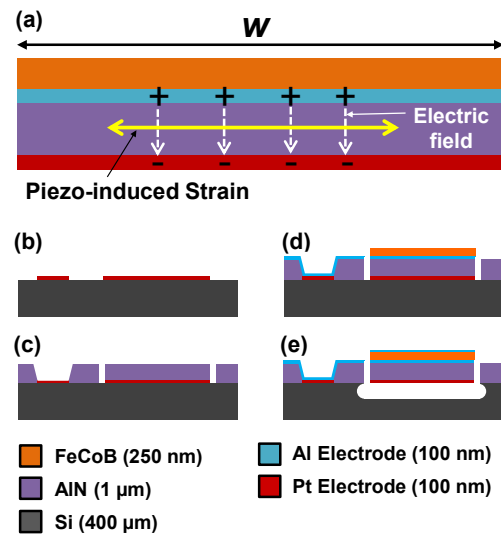


Figure 1: (a) Side view of the resonator. Fabrication starts with (b) lift off of Pt bottom electrode, and then (c) AlN layer deposition followed by via and release etch hole formation with chlorine based RIE. (d) FeCoB layer deposition and (e) XeF<sub>2</sub> release etch completes the device fabrication.

Figure 1(b-e) show device fabrication flow that consists of a 4-mask process. First, a 100-nm-thick Pt bottom electrode is patterned by photolithography followed by a 1- $\mu\text{m}$ -thick AlN sputter deposition. To form electrical via to the bottom electrode and release etch holes two separate steps of chlorine based RIE are performed. An in-situ H-field of 20 Oe was applied during the FeCoB deposition in order to orient the EZ of the sensor. In addition, the sputtering temperature was closely monitored to be below 70 °C to deposit an amorphous film of FeCoB. The FeCoB to AlN thickness ratio was selected as a trade-off between sensor sensitivity and resonator  $Q$  and  $k_t^2$ . Next, a 10-nm-thick Al layer was deposited to protect FeCoB during the device release. Finally, XeF<sub>2</sub> Si etch releases the resonator and completes the device fabrication.

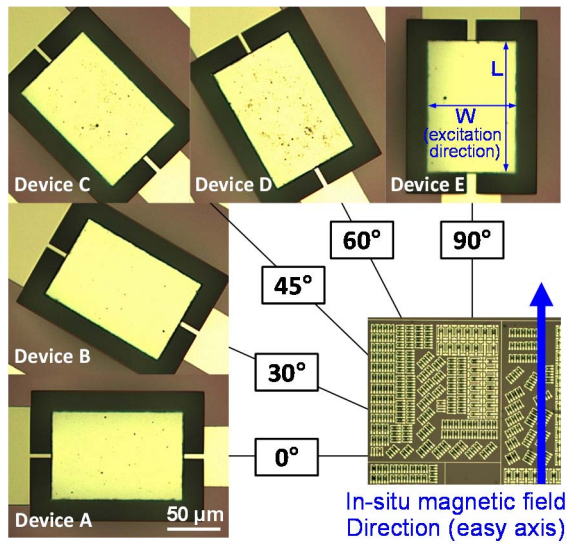


Figure 2: (a) Image of 43 MHz resonator sensor array with different excitation directions ( $\theta = 0 \sim 90^\circ$ ) with respect to the fixed easy axis (EZ) of a pre-magnetized FeCoB film.

To synthesize a single-chip multi-axis sensor, an array of five 43 MHz resonators ( $w = 90 \mu\text{m}$ ) vibrating along different  $\theta$ s ranging from  $0^\circ$  to  $90^\circ$  with respect to the EZ is used to attain angular information of H-field, as shown in Figure 2. Delta-E effect depends not only on the magnitude of H-field, but also on the angle between H-field and EZ. Theoretically, delta-E is largest when H-field is vertical to EZ, since it induces the largest rotation of magnetic domains. Our sensor array design allows further investigation to understand the correlation between the resonator excitation orientation and delta-E effect of the integrated FeCoB layer.

Figure 3 shows the measured admittance and phase as a function of frequency and their modified Butterworth-Van dyke (mBVD) model fitting. The measured  $Q$  (3dB) and  $k_t^2$  are about 1558 and 2%, respectively, giving a high figure of merit ( $\text{FOM} = Q \cdot k_t^2$ ) exceeding 30. This FOM value is about 2.5X improvement compared to state-of-the-art PM-MRS [6]. In addition, the use of Al as a top electrode instead of FeCoB, lowered the series resistance ( $R_s$ ) of the device compared to aforementioned PM-MRS.

Resonators with identical parameters but without a FeCoB layer were fabricated on the same chip and demonstrated higher  $Q$ s of about 2000, indicating that the layer of FeCoB could be the source of additional damping.. Hence, the materials composition of PM-MRS should be carefully designed to balance the measurement sensitivity and resonator properties, such as  $Q$  which directly impacts the flicker noise of AlN MEMS resonators [10].

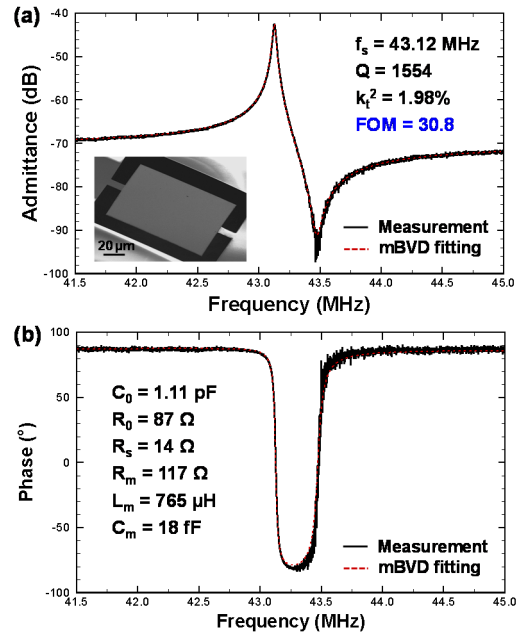


Figure 3: Measured (a) admittance and (b) phase and their modified Butterworth-Van Dyke (mBVD) model fitting. ( $C_0$ : resonator capacitance,  $R_0$ : resonator resistance,  $R_s$ : series resistance,  $R_m$ : motional resistance,  $L_m$ : motional inductance,  $C_m$ : motional capacitance)

## EXPERIMENTAL RESULTS AND DISCUSSION

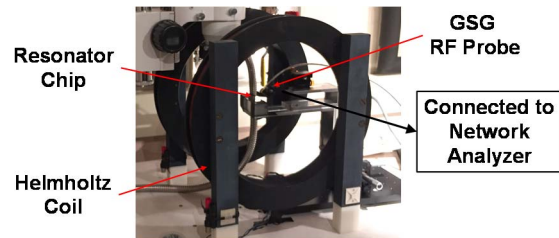


Figure 4: Measurement setup. Admittance response is directly measured using a network analyzer.

Figure 4 shows the resonator measurement setup under H-field. Using a network analyzer, the admittance response of a PM-MRS was monitored versus H-field generated by a Helmholtz coil. The coil generates a magnetic field of up to 100 Oe, which is above the saturation H-field for delta-E effect of FeCoB. The measurement temperature was at about  $20 \pm 0.5$  °C. Since the temperature coefficient of frequency

(TCF) of AlN resonators (tens-of-ppm/°C) is comparable to the measurement sensitivity of a PM-MRS, temperature was closely monitored throughout the experiment.

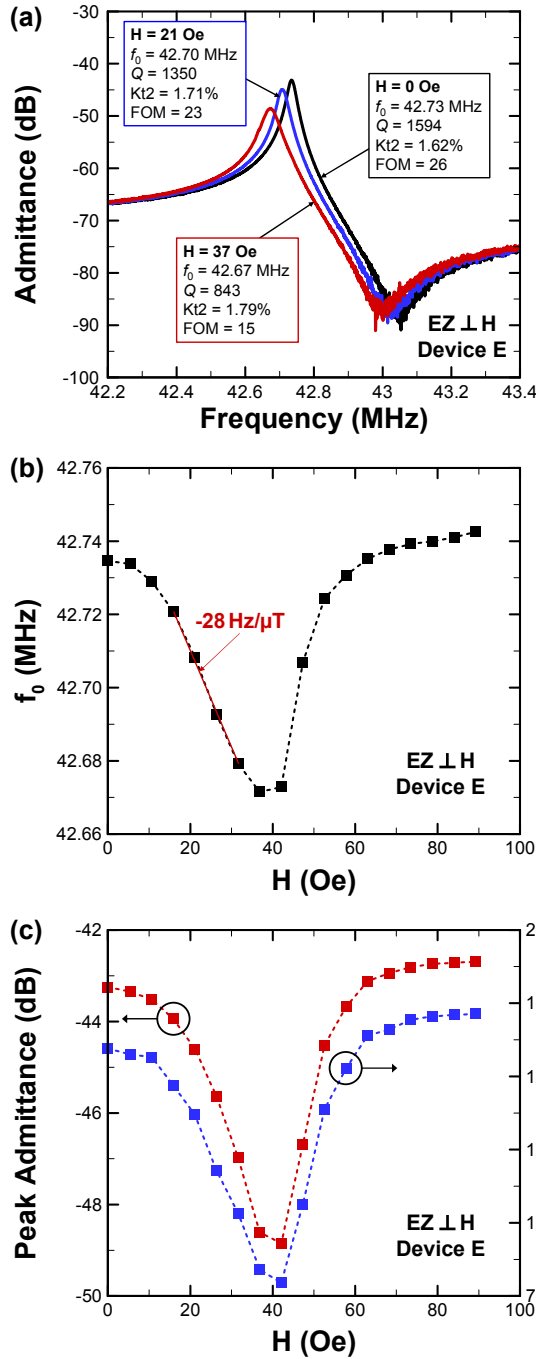


Figure 5: (a) Measured admittance response of a resonator at various H-field magnitudes. (b-c)  $f_0$ , peak admittance, and  $Q$  changes as a function of H-field, enabling a high precision magnetic field detection. When  $H$  is above 60 Oe,  $E$  of FeCoB saturates and changes in resonator response become small.

Figure 5 shows a response of device E when the H-field is applied perpendicular to EZ (or along the excitation direction). Figure 5(a) shows a measured admittance

response at three different H-field magnitudes of 0, 21, and 37 Oe; it is clearly shown that  $f_0$ ,  $Q$ , and peak admittance all depend on the magnitude of H-field. For further analysis, the admittance response of a resonator is monitored at a wider H-field range of from 0 to 90 Oe. Figure 5(b-c) show that  $f_0$ , peak admittance, and  $Q$  are a function of the applied H-field. In lower H-field regime (0 ~ 40 Oe),  $f_0$  decreases as FeCoB becomes softer due to the magnetic domain rotation. As domains rotate and align with the applied H-field,  $E$  of FeCoB, as well as  $f_0$ , increase and eventually saturate at a H-field magnitude of about 60 Oe. The measurement sensitivity is about -28 Hz/μT in a H-field range of from 16 to 32 Oe. For the remainder of this paper, we monitor the change in  $f_0$  ( $\Delta f_0$ ) for simplicity. However, tracking the amplitude modulation could give higher measurement sensitivity as the overall normalized shift in peak amplitude is larger than  $\Delta f_0$ .

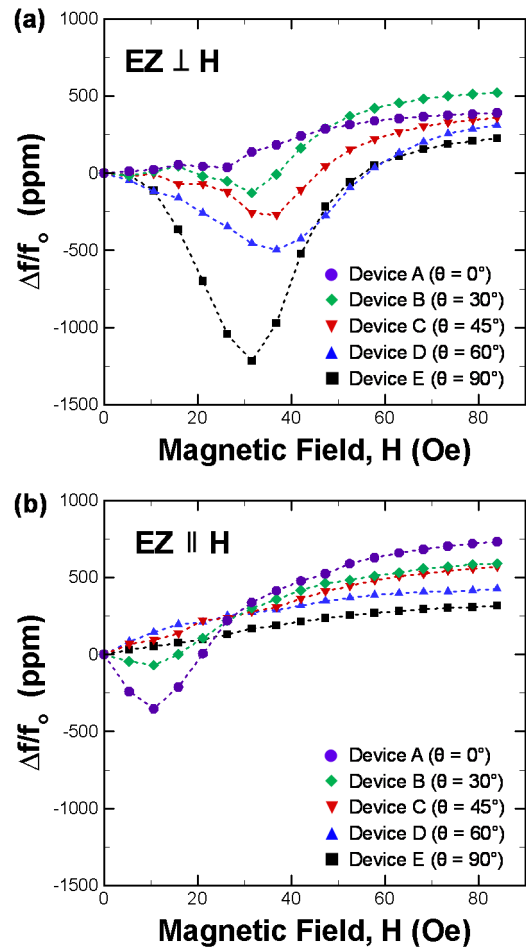


Figure 6: Shift in resonant frequency ( $\Delta f/f_0$ ) for different  $\theta$  as a function of  $H$  when a)  $H$  is orthogonal to the EZ axis and b)  $H$  is parallel to the EZ axis. For both cases, the magnitude of  $\Delta f/f_0$  is largest when  $H$  is along the excitation direction of the resonator.

For multi-axis H-field detection, we measured  $f_0$  of each resonator in the array for two different directions of H-field with respect to EZ at  $0^\circ$  and  $90^\circ$ , as shown in figure 6. For

both cases,  $\Delta f/f_0$  is largest when the direction of H-field is along the resonator excitation direction. This data show that not only delta-E effect, but also the resonator excitation direction plays a key role in H-field detection. In addition,  $\Delta f/f_0$  is larger when H-field is orthogonal to EZ as the rotation of the magnetic domains is larger, which means higher delta-E effect. Figure 7 shows  $\Delta f/f_0$  of each resonator at two different directions of H-field at 37 Oe. As expected, the change in  $f_0$  increases with  $\theta$  for both H-field directions. Combining  $\Delta f/f_0$  information of each resonator in an array would allow an accurate measurement of not only H-field magnitude, but also its direction. Moreover, some of the devices in the array are sensitive up to H-field of about 90 Oe, further increasing the dynamic range of the sensor.

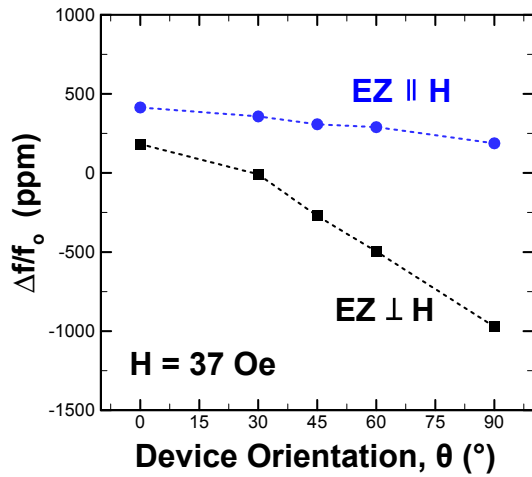


Figure 7:  $\Delta f/f_0$  of each resonator at H of about 37 Oe with different angles between H and EZ. The range of  $\Delta f/f_0$  is larger when H is orthogonal to the EZ axis.

Our sensor array allows a high resolution detection of H-field orientation and its magnitude over a wide range of values going from 0 to 90 Oe. However, there are several key challenges to overcome before this technology could be considered as a substitute for commercial magnetometers. First, PM-MRS cannot accurately detect the sign (+/-) of H-field, because the delta-E effect is a function of the absolute value of H-field magnitude. Self-biasing via pre-magnetization allows PM-MRS to distinguish the sign of H-field, but this approach limits the dynamic range of the sensor [6]. In addition, our PM-MRS gives the highest measurement sensitivity for a H-field ranging from 10 to 40 Oe, but lower sensitivity near zero H-field. Although an external magnetic bias would enable not only maximum sensitivity, but also directionality (distinguishing +/-) near zero H-field (i.e. earth magnetic field of  $\sim 0.5$  Oe), this solution will come at the expenses of either greater power consumption or larger footprint (assuming an external magnet is used). Lastly, our sensor array currently lacks the ability to detect out-of-plane (z-oriented) H-field. Further device design optimization and materials engineering is required to realize 3-axis MEMS magnetometers using piezoresistive / magnetorestrictive composites in a single chip.

## CONCLUSION

We demonstrate an array of integrated PM-MRS with different excitation orientations for in-plane multi-axis magnetic field detection. Each resonator exhibits unique mechanical and electrical responses as a function of H-field magnitude and its direction, with a maximum measurement sensitivity of about  $-28$  Hz/ $\mu$ T. Fabricated resonators give high  $Q$ s of about 1500 and  $k_t^2$  around 2%, resulting in a figure of merit exceeding 30 – the highest value reported for AlN based PM-MRS. This sensor array could enable ultra-low power and ultra-low noise MEMS magnetometers for future wireless sensing and navigation applications.

## ACKNOWLEDGEMENTS

This work was supported by CMU-SYSU CIRC.

## REFERENCES

- [1] H. D. Nguyen *et al.*, "UHF piezoelectric quartz mems magnetometers based on acoustic coupling of flexural and thickness shear modes," *28th IEEE International Conference on MEMS*, 2015, pp. 944-947.
- [2] V. Kumar *et al.*, "Lorentz force MEMS magnetometer with frequency modulated output," *IEEE 29th International Conference MEMS*, 2016, pp. 589-592.
- [3] G. Laghi *et al.*, "100  $\mu$ A, 320 nT/Hz $^{1/2}$ , 3-AXIS Lorentz force MEMS magnetometer," *18th International Conference on Solid-State Sensors, Actuators and Microsystems (TRANSDUCERS)*, 2015, pp. 803-806.
- [4] S. Sonmezoglu *et al.*, "Force-rebalanced Lorentz force magnetometer based on a micromachined oscillator," *Applied Physics Letters*, vol. 106, p. 093504, 2015.
- [5] G. Hatipoglu and S. Tadigadapa, "Micromachined magnetoflexoelastic resonator based magnetometer," *Applied Physics Letters*, vol. 107, p. 192406, 2015.
- [6] Y. Hui *et al.*, "High Resolution Magnetometer Based on a High Frequency Magnetolectric MEMS-CMOS Oscillator," *Journal of Microelectromechanical Systems*, vol. 24, pp. 134-143, 2015.
- [7] S. Zabel *et al.*, "Phase modulated magnetolectric delta-E effect sensor for sub-nano tesla magnetic fields," *Applied Physics Letters*, vol. 107, p. 152402, 2015.
- [8] B. D. Cullity, "Introduction to Magnetic Materials," Addison-Wesley Publishing Company, 1972.
- [9] J. M. Barandiarán *et al.*, "Influence of annealing temperature on the magnetic and magnetoelastic properties in Fe-Co-B metallic glasses," *Journal of Non-Crystalline Solids*, vol. 329, pp. 43-47, 2003.
- [10] H. J. Kim, J. Segovia-Fernandez, and G. Piazza, "Damping directly impacts flicker frequency noise of piezoelectric aluminum nitride resonators," *IEEE 29th International Conference on MEMS*, 2016, pp. 667-670.

## CONTACT

- \*H.J. Kim: +82-10-3691-1307; kim.hoejoon@gmail.com
- \*J. Zhu: +1-412-268-8523; jingxiz@andrew.cmu.edu
- \*G. Piazza: +1-412-268-7762; piazza@ece.emu.edu